Non-Empirical Energetic Analysis of Reactivity and Covalent Inhibition of Fatty Acid Amide Hydrolase.

ARTICLE *in* THE JOURNAL OF PHYSICAL CHEMISTRY B · MAY 2013

Impact Factor: 3.3 · DOI: 10.1021/jp401834v · Source: PubMed

8 AUTHORS, INCLUDING:

Edyta Dyguda-Kazimierowicz
Wroclaw University of Technology
14 PUBLICATIONS **201** CITATIONS
SEE PROFILE

Waclaw Andrzej Sokalski
Wroclaw University of Technology
119 PUBLICATIONS **2,355** CITATIONS
SEE PROFILE

Alessio Lodola
Università degli studi di Parma
85 PUBLICATIONS **1,443** CITATIONS
SEE PROFILE

Marco Mor
Università degli studi di Parma
183 PUBLICATIONS **6,004** CITATIONS
SEE PROFILE

THE JOURNAL OF PHYSICAL CHEMISTRY B

Article

pubs.acs.org/JPCB

Nonempirical Energetic Analysis of Reactivity and Covalent Inhibition of Fatty Acid Amide Hydrolase

Ewa I. Chudyk,[†] Edyta Dyguda-Kazimierowicz,[‡] Karol M. Langner,[‡,∥] W. Andrzej Sokalski,*[,‡] Alessio Lodola,[§] Marco Mor,[§] Jitnapa Sirirak,[†] and Adrian J. Mulholland*[,†]

[†]Centre for Computational Chemistry, School of Chemistry, University of Bristol, Bristol, BS8 1TS, United Kingdom

[‡]Institute of Physical & Theoretical Chemistry, Wrocław University of Technology, 50-370 Wrocław, Poland

[§]Dipartimento Farmaceutico, Università degli Studi di Parma, 43100 Parma, Italy

[∥]Department of Molecular Physiology and Biological Physics, University of Virginia, Charlottesville, VA 22908, USA

Supporting Information

ABSTRACT: Fatty acid amide hydrolase (FAAH) is a member of the amidase signature family and is responsible for the hydrolytic deactivation of fatty acid amide neuromodulators, such as anandamide. FAAH carries an unusual catalytic triad consisting of Lys-Ser-Ser, which uniquely enables the enzyme to cleave amides and esters at similar rates. The acylation of 9*Z*-octadecenamide (oleamide, a FAAH reference substrate) has been widely investigated by computational methods, and those have shown that conformational fluctuations of the active site affect the reaction barrier. Empirical descriptors have been devised to provide a possible mechanistic explanation for such conformational effects, but a first-principles understanding is still missing. A comparison of FAAH acylation with a reference reaction in water suggests that transition-state stabilization is crucial for catalysis because the activation energy barrier falls by 6 kcal/mol in the presence of the active site. With this in mind, we have analyzed the enzymatic reaction using the differential transition-state stabilization (DTSS) approach to determine key active-site residues for lowering the barrier. We examined several QM/MM structures at the MP2 level of theory and analyzed catalytic effects with a variation−perturbation partitioning of the interaction energy into electrostatic multipole and penetration, exchange, delocalization, and correlation terms. Three residues − Thr236, Ser218, and one water molecule − appear to be essential for the stabilization of the transition state, a conclusion that is also reflected by catalytic fields and agrees with site-directed mutagenesis data. An analogous analysis for URB524, URB618, and URB694 (three potent representatives of covalent, carbamate-based FAAH inhibitors) confirms the importance of the residues involved in oleamide acylation, providing insight for future inhibitor design.

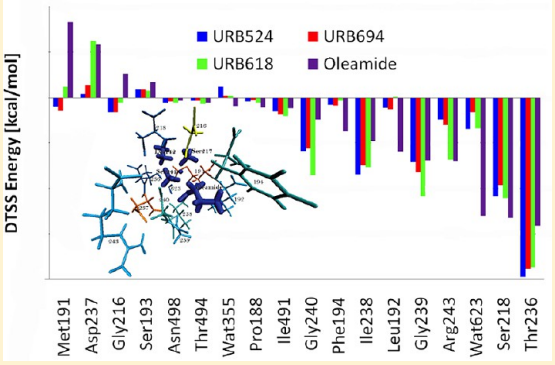

INTRODUCTION

Enzymes are highly effective catalysts and accelerate most of the reactions proceeding inside living organisms. Among several available explanations of this fact, the most influential has been Pauling's transition-state stabilization hypothesis,[1] which states that enzymes bind the transition state (TS) more strongly than reactants and therefore lower the activation energy barrier. Such selectivity may involve structural flexibility and specific electrostatic interactions within the active site because the catalytic environments of enzymes tend to be preorganized toward the stabilization of the TS.[2,3] Regardless of the molecular details, the first step in understanding the molecular basis of enzymatic activity is to determine essential active site residues, information that should also prove to be useful for inhibitor design.

Fatty acid amide hydrolase (FAAH) is a member of the amidase signature (AS) family,[4] with a catalytic Lys-Ser-Ser triad responsible for the hydrolytic deactivation of the endogenous fatty acid amide family of signaling lipids.[5] The main substrate of FAAH is probably the endocannabinoid anandamide (arachidonoylethanolamide), which activates specific cannabinoid receptors found in the brain and in immune cells and which is essential for the regulation of pain, anxiety, and memory.[6−8] Other potential substrates are also known: palmitoylethanolamide (involved in anti-inflammatory processes),[9] oleoylethanolamide (a satiety factor),[10] and oleamide (associated with inducing sleep).[11−13] Because of these central functions in living organisms, FAAH has been investigated extensively both experimentally and computationally.[14]

Several crystal structures of FAAH have been deposited in the Protein Data Bank, and the one most widely employed in

Received: February 21, 2013
Revised: May 3, 2013
Published: May 8, 2013

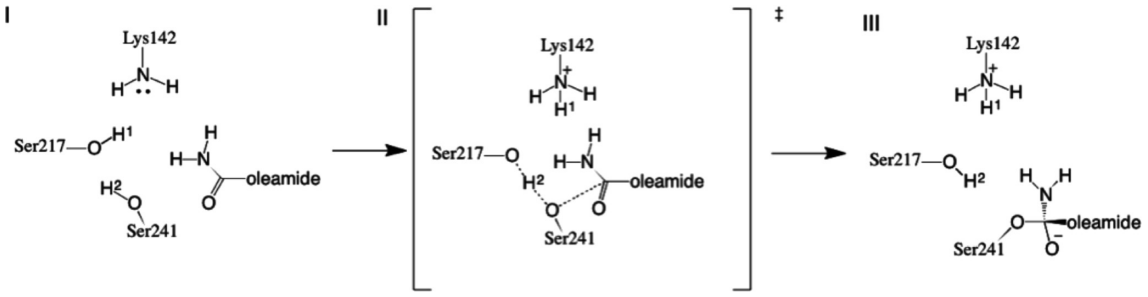

Figure 1. Proposed mechanism of FAAH acylation[23,16] proceeds from the Michaelis complex (I) through the transition state (II) up to the tetrahedral intermediate (III). In the reactant state, both catalytic serines (Ser217 and 241) are protonated, while Lys142 is neutral. A second proton transfer involving H^2 accompanies the first, Ser217-assisted one. The highest energy configuration is attained in QM/MM calculations[17] when H^2 is almost equidistant between Ser241 and Ser217 and the oleamide is halfway to Ser241. The tetrahedral intermediate is formed subsequently.

modeling is a covalent adduct with methyl arachidonylfluorophosphonate (PDB code: 1mt5).[15] This particular structure has been used by several research groups for mechanistic investigations[16−20] and deriving structure−activity relationships.[21,22] It is the Lys142-Ser217-Ser241 catalytic triad mentioned above that is responsible for the remarkable ability of FAAH to hydrolyze amides and esters at similar rates, by mechanisms in which acylation is the rate-limiting step.[23] The catalytic mechanism of FAAH involves the formation of a tetrahedral intermediate (TI) after a nucleophilic attack of the catalytic Ser241 on the carbonyl group of the substrate (Figure 1). This reaction involves a double proton transfer, in which neutral Lys142 cooperates with Ser217 to deprotonate Ser241. The TI is a transient configuration along the reaction pathway, and its collapse, triggered by the Lys142-aided protonation of the leaving group, releases a free amine and causes an enzyme-bound acyl intermediate to form.[23]

Site-directed mutagenesis offers the most direct evidence that the Lys142-Ser217-Ser241 triad is crucial and suggests other key amino acid residues for FAAH-assisted reactions on substrates such as oleamide and oleoyl methyl ester.[24,23,25,26] Mutating any residue in the catalytic triad to Ala decreases FAAH oleamide hydrolysis activity to below 0.1% of the wild type and to between 3 and 0.3% for ester hydrolysis. The oleamide reaction is also strongly influenced by residues Arg243 and Ser218, and their replacement by Ala reduces FAAH activity to 0.3 and 1%, respectively.[24] The apparent wild-type activation energy barrier (calculated from experimental reaction rates using Eyring equation), which is around 16.1 to 16.7 kcal/mol for oleamide hydrolysis,[23,26] grows accordingly after such mutations; the strongest effect has been observed following the Ser241Ala mutation, which increases it to 25 kcal/mol.[26] A number of Lys142 mutations (Lys142Ala, Lys142Ala/Ser217Ala, and Lys142Glu) also all raise the barrier height, albeit to 22.1 to 22.8 kcal/mol,[23,25] and the Ser217Ala mutation to 20.9 to 21.3 kcal/mol.[23,26] The impact of Ser218 is slightly smaller, and the Ser218Ala mutation leads to an apparent barrier of 19.4 kcal/mol.[26]

In previous studies conducted in our group, the catalytic mechanism of FAAH with oleamide was investigated by hybrid quantum-mechanics/molecular-mechanics (QM/MM) methods.[16,17] Both semiempirical (PM3-CHARMM22) and density functional theory (B3LYP/6-31+G(d)//PM3-CHARMM22) calculations indicated that the nucleophilic attack of Ser241 on oleamide is a key event in the acylation reaction. Subsequent molecular dynamics simulations provided four representative starting structures (called A, B, C, and D), and the corresponding reaction pathways exhibited significantly different activation energies (28, 33, 29, and 18 kcal/mol, respectively). The pathway originating from conformation D was found to have the lowest activation barrier, in good agreement with the experimental value. Therefore, we surmised that conformation D is the reactive one and that it is reached through fluctuations of the enzyme active site.[15,18] The QM/MM calculations indicated that the difference in the barrier was due to better TS stabilization in the conformation D. Molecular dynamics simulations suggest that it lies roughly 3 kcal/mol above the reactive conformation.

With this in mind, we investigate the barrier height for these various conformations and identify key residues using the differential transition-state stabilization (DTSS) method, which focuses on the TS stabilization energy relative to the reactants and a variation−perturbation partitioning of the interaction energy. This nonempirical analysis also provides a useful test of the QM/MM calculations. Further hints for molecular design may be obtained from catalytic fields (derived from changes in the electrostatic potential during a reaction), especially when electrostatic effects dominate interactions. This has been shown to be the case for several enzyme systems previously studied; it is the basis for models with possible applications in the design of TS analogues and alternative substrates.[27−29] The active-site model employed here enables fast and efficient analysis based on a two-body approach, which was additionally verified with a supermolecular model including many-body effects. Information about the strongest interactions in the TS might be useful for designing inhibitors that work as TS analogues.

COMPUTATIONAL METHODS

Differential Transition-State Stabilization and Its Components. The DTSS method can highlight the amino acid residues that facilitate a given reaction by comparing and monitoring the corresponding changes in activation energy that result from their presence. This change Δ for a particular residue R can be expressed as the difference between its interaction energy with the TS ($\Delta E_{TS\text{-}R}$) and substrates ($\Delta E_{S\text{-}R}$)

$$\Delta = \Delta E_{TS\text{-}R} - \Delta E_{S\text{-}R} \quad (1)$$

The magnitude of Δ measures a particular residue's catalytic activity; therefore, a negative value indicates differential TS stabilization relative to the reactants.[27]

To analyze the physical nature of interactions between active site residues and the reactive system, we partition Δ according to a variation−perturbation interaction energy decomposition scheme[30] into electrostatic multipole ($\Delta_{EL\text{-}MTP}$, representing

dx.doi.org/10.1021/jp401834v | J. Phys. Chem. B 2013, 117, 6656−6666

interactions between atomic charges, dipoles, and higher moments), electrostatic penetration ($\Delta_{EL\text{-}PEN}$), exchange (Δ_{EX}), delocalization (Δ_{DEL}), and correlation (Δ_{CORR}) terms. These components define the sequence of electrostatic (Δ_{EL}), Heitler–London (Δ_{HL}), Hartree–Fock (Δ_{SCF}), and Møller–Plesset (Δ_{MP2}) levels of theory, which form a hierarchy of interaction energies:

$$\Delta = \underbrace{\underbrace{\underbrace{\underbrace{\Delta_{EL}}_{\Delta EL} + \Delta_{HL}}_{\Delta HL} + \Delta_{SCF}}_{\Delta SCF} + \underbrace{\Delta_{EX} + \Delta_{DEL} + \Delta_{CORR}}_{\Delta MP2}}_{} \quad (2)$$

It is worth underlining here that although the more accurate levels in this analysis are more computationally demanding, they enable one to verify whether the approximate ones are reliable.[28]

Pairwise Interactions and Many-Body Effects. It can be useful to identify the most important active site residues and their individual DTSS effects, beyond the overall DTSS as outlined above. The only additive term in eq 2, however, is electrostatics, indicating in general the need for further approximations. Although the dominant role of electrostatic effects makes a system more straightforward to investigate and many literature reports have dealt with enzymatic reactions in which electrostatic interactions are dominant[3,31] (including chorismate mutase,[28] 4-methyl-5-β-hydroxyethylthiazole kinase,[32] and cAMP-dependent protein kinase A[29]), it cannot be assumed without precedent and should be verified in different cases. As active site models grow in size, the mutual polarization of residues surrounding the reaction site could become significant, which would destroy the validity of a pairwise model. Therefore, here we first calculate the effects arising from single residues making up the active site model and then apply the supermolecular approach to validate these results. All interaction energies reported here account for basis set superposition error through the counterpoise correction,[33] but basis set extension effects when changing from the pairwise to supermolecule model were not considered.

Catalytic Fields. Wherever electrostatic interactions dominate within an enzyme's active site, the molecular environment exhibiting optimal catalytic activity can generally be illustrated as the difference between the molecular electrostatic potentials of the TS and substrate S

$$\Delta = -(V^{TS} - V^{S}) \quad (3)$$

In cases where there are relatively large conformational changes during the reaction, an intermediate from the energy pathway could be considered instead of the substrate. This would then provide details of the considered step only and could be repeated analogously for other reaction steps.

To calculate catalytic fields, the electrostatic potentials for substrate and TS structures were calculated at the RHF/6-31G(d) level of theory with Gaussian09[34] software as "cube" files. Next, two other files of the same format with electron density were calculated, and the geometries of substrate and TS were aligned using a least-squares method to have the same system coordinate. The common electronic isodensity surface for the TS and substrate is found using condition $\rho_S + \rho_{TS} = 0.01$ au (ρS and ρTS stand for the electron densities of the substrate and TS, respectively) to ensure that the surface does not come too close to any of the species considered. The differential electrostatic potential was calculated as in eq 3, mapped on the isodensity surface, and visualized with VMD.[35] Values of ΔV on the isoelectronic density-surface around the reactants approximately represent the magnitude of catalytic effects that would result from appropriately positioned charged or polar residues, namely, those involved in hydrogen bonding with the TS.[28]

Multiple Sequence Alignment. The search for amino acid sequences from amidase signature family[4] members was conducted with BLAST,[36] with the rat sequence as a reference.[7] Multiple records from the same organism as well as all hypothetical, predicted, and putative records were excluded. Sequences were aligned by ClustalX[37] to distinguish the most evolutionarily conserved residues.

Active-Site Model and Calculation Details. The geometries of FAAH were taken from a previous QM/MM study[16] at the B3LYP/6-31+G(d)//PM3-CHARMM22 level of theory. On the basis of closest contacts, 16 amino acid residues and 2 water molecules were included in the active-site model. Depending on orientation with respect to the reaction center, either entire amino acid residues or only their side chains/backbones were extracted from the initial structure and capped with hydrogen atoms, which in turn were optimized at the HF/6-31G level of theory using Gaussian03.[34] The same procedure and active-site model were used for DTSS calculations with the URB524, URB694, and URB618 inhibitors, which incorporated the inhibitor instead of oleamide in the reaction center.

The catalytic triad (Lys142-Ser217-Ser241) and oleamide up to the C4 carbon atom comprised the reaction center, totaling to 34 atoms. Interaction energies between the reaction system and each separate residue (pairwise calculations) or the entire active site model (supermolecular approach) were performed with the 6-31G(d) basis set using a modified version of GAMESS-US,[38,39] allowing for the decomposition of the interaction energy into the components described above. The electron density and electrostatic potential data employed in the catalytic field derivation were calculated at the RHF/6-31G(d) level of theory and visualized using the VMD package.[35]

RESULTS AND DISCUSSION

Reference Water System for the Reaction in FAAH. The catalytic power of an enzyme becomes evident when one contrasts a reaction proceeding in water and in the active site. Therefore, we start by comparing the catalytic power of FAAH to the uncatalyzed reference reaction in solution. Following a thermodynamic cycle,[3] the reaction starts with a neutral Lys142 (instead of in a protonated state, favorable in solution) and proceeds in the same manner as in the enzyme. The difference between an activation energy barrier in the enzyme and in water arises from interactions with the environment, and these are lower in the enzyme, whose active site is preorganized to stabilize the TS.[3,40] The aim of these calculations is to investigate the role of the protein environment rather than explore the regular reaction mechanism in water.

The lowest reaction energy pathway (conformation D) was extracted from the potential energy surface of the reactive conformation described in refs 15 and 16. For selected snapshots along the reaction coordinate in the enzyme, 34 QM atoms representing the reaction center were used for reference calculations in water. The coordinates of these atoms

dx.doi.org/10.1021/jp401834v | J. Phys. Chem. B 2013, 117, 6656–6666

were unchanged, and single-point calculations at the B3LYP/6-31+G(d) level were performed using PCM water as a reaction environment. The resulting potential energy profile (Figure 2)

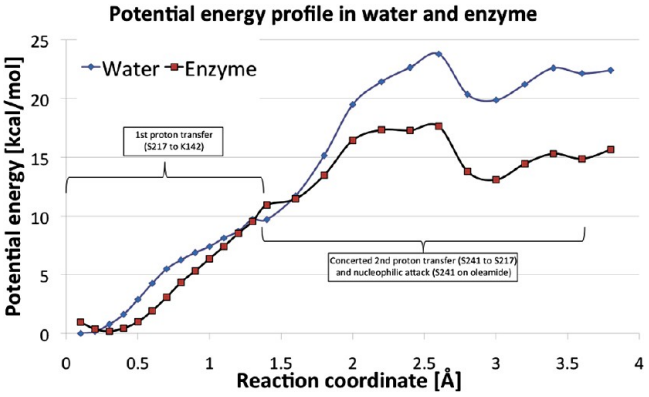

Figure 2. Potential energy profile of tetrahedral intermediate formation in the enzyme (B3LYP/6-31+G(d)//PM3-CHARMM22)[16,17] and in water. The reference reaction in water was modeled simply by taking the structures of the QM region from QM/MM calculations on the enzyme and performing PCM implicit solvent calculations at the B3LYP/6-31+G(d) level of theory. Symbols show calculated data points.

has an overall shape similar to that in the enzyme: the energy of the first proton transfer is slightly lower in water (9.5 instead of 11 kcal/mol) and much higher for the second phase (24 compared with 18 kcal/mol for the enzyme). The barrier in enzyme is lowered by the specifically positioned toward TS active-site residues, whereas in water the stabilization at the reactant and TSs is similar. The stabilizing power of FAAH is clearly concentrated in the second phase of the reaction, comprising a concerted proton transfer between Ser241 and Ser217 and a nucleophilic attack of Ser241 on oleamide. The final energy at the tetrahedral intermediate relative to the reactants is 15 and 22 kcal/mol for the reaction in the enzyme and in water, respectively, which is a comparable change relative to the TS. This reference profile in water is also in agreement with a B3LYP/aug-cc-pVDZ profile for the methanolysis of formamide published elsewhere,[40] obtained for a model system for serine proteases. The activation energy barrier in that case, in solution with ammonia as the general base, is 24 kcal/mol, consistent with the experimental value.

DTSS Effects. A DTSS analysis was performed for each of the four conformations (A, B, C and D) from ref. [17], revealing the contributions of active site components (Figure 3 and Tables SI-1 − SI-4 in Supporting Information) and illustrating why different conformations lead to different barriers. As seen in Table 1, the B3LYP activation energy barriers correlate roughly linearly with the sum of two-body DTSS contributions from each residue-reaction center pair. The reactive conformation D, with the lowest activation energy, also exhibits the strongest DTSS effects, while the weakest DTSS is associated with the highest barrier (structure B). The larger spread in activation energies reflects additional energy differences between the various TSs (the structures of the reacting system differ), whereas DTSS accounts only for intermolecular interactions (between the reacting system and its environment). Nevertheless, both energies yield the same ordering of pathways.

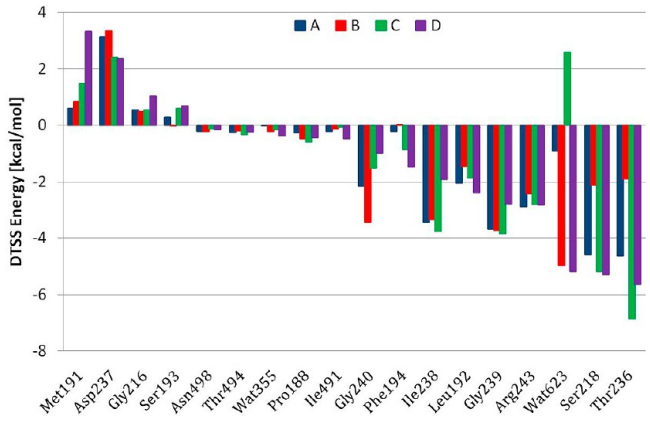

Figure 3. DTSS effects calculated at the MP2 level of theory for conformations A, B, C, and D taken from ref 17. FAAH active-site components (residues and water molecules) are ranked in order of increasing contributions to differential TS stabilization for the reactive conformation D.

Table 1. B3LYP//PM3-CHARMM22 Activation Energy Barriers from Ref 17 and the Corresponding MP2 Differential Transition-State Stabilization Energy[a]

ID	activation energy[17]	DTSS
A	28	−20.92
B	33	−19.90
C	29	−20.29
D	18	−22.74

[a]All energies are given in kilocalories per mole.

For all four conformations, the same residues were found to be important for stabilizing the TS in the first acylation step: Thr236, Ser218 (caging residues around Lys142), Leu192, Phe194 (substrate binding), Ile238, Gly239, Gly240 (oxyanion hole), Wat623, and Arg243. Several destabilizing amino acid residues were identified, including Met191, Asp237, Gly216, and Ser193. While the role of stabilizing residues is to facilitate tetrahedral intermediate formation, the destabilizing ones also appear to be important for the overall reaction, as they might aid further reaction steps (leaving group expulsion or deacylation) and influence the energetic equilibrium or product release. There are some minor differences between the four considered conformations (Figure 3). For example, Wat623 in conformation C exhibits significant destabilizing effects due to its opposite orientation in the FAAH active site compared with the other structures. In conformations A, B, and D it forms a hydrogen bond with Ser217 and Ser241 during the second proton transfer, whereas in conformation C this water molecule is rotated with hydrogen atoms pointing in different directions, leading to slightly destabilizing interactions between Wat623 and the serine residues involved in the reaction.

Of special interest is the reactive conformation D (the entire active site model for this conformation is presented in Figure 4), which likely provides the best representation of interactions during TI formation and the largest TS stabilization. Residues that lower the activation energy barrier the most are: Thr236 (−5.6 kcal/mol), Ser218 (−5.3 kcal/mol), Wat623 (−5.2 kcal/mol), Arg243 (−2.8 kcal/mol), Gly239 (−2.8 kcal/mol), Leu192 (−2.4 kcal/mol), Ile238 (−1.9 kcal/mol), Phe194 (−1.5 kcal/mol), and Gly240 (−1.0 kcal/mol). Destabilizing

dx.doi.org/10.1021/jp401834v | J. Phys. Chem. B 2013, 117, 6656−6666

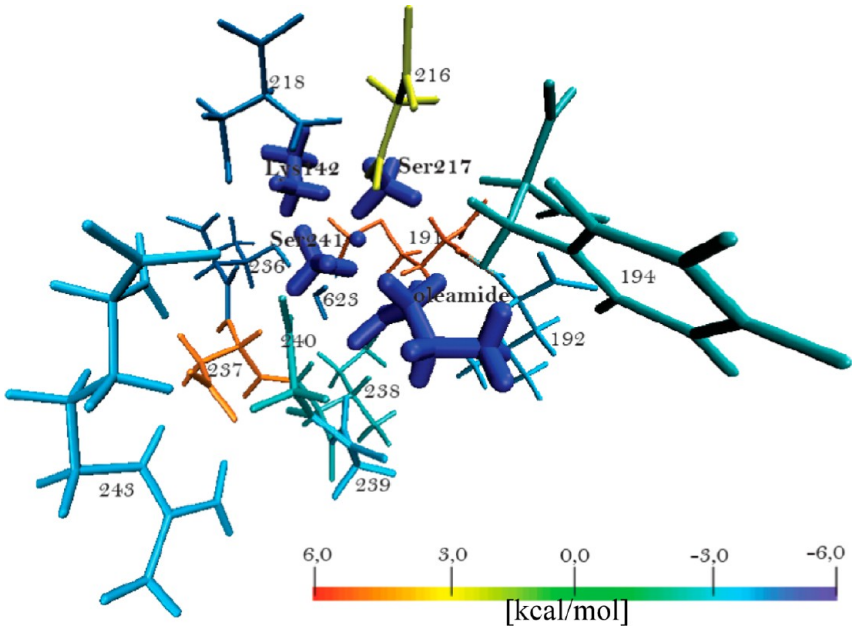

Figure 4. Structure of the FAAH active site at the transition state for the reactive conformation D of oleamide acylation. The coloring scheme applied to active site components reflects their contribution to differential transition-state stabilization (blue colors represent stabilizing and yellow to red represent destabilizing effects). The reaction center subsystem, including the Lys142-Ser217-Ser241 triad, is shown as a dark-blue thick stick.

effects are exerted by Met191 (3.3 kcal/mol), Asp237 (2.4 kcal/mol), Gly216 (1.0 kcal/mol), and Ser193 (0.7 kcal/mol).

Residues that lower the activation energy barrier (Thr236 and Ser218) stabilize the first proton transfer by forming hydrogen bonds with Lys142, which becomes positively charged in that stage. The backbone atoms of Gly239, Ile238, and Gly240 (along with Ser241 are not analyzed here) form an oxyanion hole, and their role is to stabilize the negative charge that builds up on the oleamide oxygen during tetrahedral intermediate formation. The role of the two ionizable residues in the reaction environment, Arg243 and Asp237, is connected to the concerted second proton-transfer and nucleophilic attack step.[17] Because they are located just behind the oxyanion hole, these two residues enhance attractive (Arg243) and repulsive (Asp237) interactions with the negatively charged oleamide oxygen in the tetrahedral intermediate. Apart from interacting with oleamide, they interact with each other, partially canceling out each others' effects (Figure 5). The role of Met191, which slightly destabilizes the tetrahedral intermediate, might be connected to a further step of oleamide hydrolysis, such as ammonia abstraction. The backbone oxygen atom forms a hydrogen bond with the amino group of the substrate.

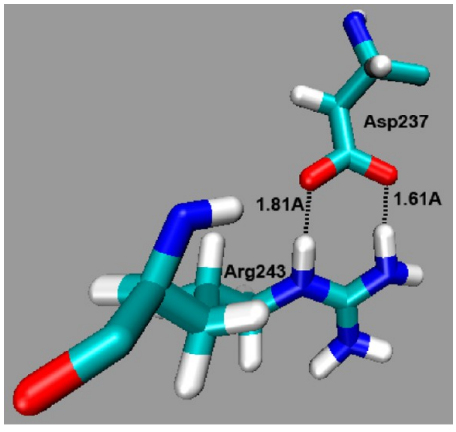

Figure 5. Hydrogen-bond distance interactions Arg243 and Asp237 (taken from the structure of conformation D[17]).

These results are consistent with a number of experimental mutagenesis studies of oleamide hydrolysis. In particular, several of the FAAH residues included in our DTSS analysis have been experimentally substituted, yielding enzymes with 1, 12, 2.3, and 0.3% of the wild-type catalytic activity for mutations Ser218A, Asp237Glu, Asp237Asn, and Arg23Ala, respectively.[23] The importance of Ser218 is also reflected by an increase in the activation energy barrier to 19.4 kcal/mol for the Ser218Ala mutant[26] compared with 16.1 to 16.7 kcal/mol[23,26] for the wild type.

Physical Nature of Interactions within the FAAH Active Site. In addition to identifying the catalytically active amino acid residues, another important issue is analyzing their interactions (Figure 6 and Tables SI-1−SI-4 in the Supporting Information). Components of the interaction energy obtained from the variational−perturbational decomposition scheme define a hierarchy of approximations (eq 2). Successive corrections, from the electrostatic penetration term up to the most expensive correlation component, tend to compensate, suggesting that the electrostatic multipole term might be the best approximation requiring the lowest computational cost. This hypothesis is also substantiated by the correlation between interaction energy calculated at subsequent levels of theory and the reference MP2 stabilization energy. Within the reactive conformation D, the corresponding correlation coefficients for the electrostatic multipole, first-order electrostatic, Heitler-London, and Hartree−Fock levels of theory are 0.97, 0.87, 0.87, and 0.99, respectively. Of these, Δ_{SCF} is the closest to Δ_{MP2}, showing that the HF result is useful and omitting correlation effects yields substantial computational savings. Calculation of Δ_{SCF} appears relatively accurate and computationally efficient. Analogous results were obtained for the remaining, unreactive conformations (Tables SI-1−SI-4 in the Supporting Informa-

dx.doi.org/10.1021/jp401834v | J. Phys. Chem. B 2013, 117, 6656−6666

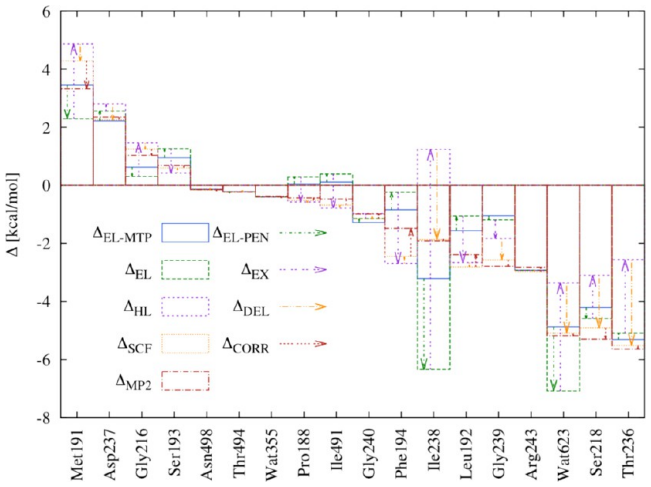

Figure 6. Components of the DTSS energy calculated according to the variation–perturbation interaction energy decomposition scheme. Horizontal lines represent energy values at successive levels of theory (with colors explained in the legend), while vertical arrows correspond to individual terms. All values are given in kilocalories per mole.

tion), confirming the essentially electrostatic nature of FAAH active-site interactions.

Validation of the Pairwise Model. The active site of an enzyme consists of multiple amino acid residues interacting with each other, and the analysis considered above based on pairwise interactions might not be accurate enough to describe the forces that govern catalysis. Therefore, another point of interest is the mutual polarization of residues, which can be evaluated by including all interacting active site residues in one calculation. To limit the size of the system, for this test, the five FAAH residues with the smallest contributions according to the dimer-based model were omitted (Asn498, Thr494, Wat355, Pro188, and Ile491). This is a significant reduction for ab initio methods, and still over 200 atoms and more than 1500 atomic orbitals were used in the final supermolecule calculations.

A comparison of supermolecule interaction energies with those obtained from summed dimer models is presented in Table 2. The DTSS results for both models have similar values at all levels of theory, implying that mutual polarization can be neglected in the FAAH active site and validating the pairwise model used.

Another important conclusion from Table 2 is that DTSS at both the Hartree–Fock level (Δ_{SCF}) and its electrostatic component (Δ_{EL}) are close to the more theoretically complete MP2 result (Δ_{MP2}). While this is not true for the interaction energies themselves, catalytic effects are determined by the difference between enzyme–substrate and enzyme–TS interaction energies (DTSS). This implies that even though electron correlation and other effects may contribute a significant portion of the absolute interaction energy, especially in the case of individual residues, they change to a much smaller extent during the reaction and therefore they do not determine the catalytic action of the surroundings.

Catalytic Field Approach. The electrostatic nature of interactions within the FAAH active site allows the catalytic field approach[27] to be used. Figure 7 shows a mapping of the differential electrostatic potential onto the electronic isodensity surfaces surrounding the reaction centers of each of the four conformations. Apparently, the most pronounced difference in charge distribution is associated with proton transfer to Lys142. According to the catalytic field results, a negatively charged environment would be optimal there, as represented by the red color around the catalytic triad (Figure 7). The same observation can be made for the oleamide part containing nitrogen atoms, in contrast with the blue region around the oxygen atoms of oleamide and the two serine residues of the catalytic triad. As indicated by the white regions, the rest of the aliphatic oleamide chain does not exhibit any significant electronic redistribution during the reaction.

The catalytic fields shown in Figure 7 reveal certain differences between the differential electrostatic potentials around the reaction centers of the four considered conformations. In particular, the charge exchange area of the Lys142 residue in conformation B shows a much less negative environment than the A, C, and D structures. Also, the areas corresponding to oleamide's nitrogen atoms are not always strongly colored, for example, for conformation C, where the differential potential becomes almost neutral. Such differences in catalytic fields probably are associated with the different DTSS effects found for the respective enzymatic environments. (See Table 1.)

In terms of inhibitor design, the reactive conformation is the most important one; therefore, the correlation between its catalytic field and crucial residues determined by DTSS was analyzed in more detail (Figure 8). The strongest electrostatic potential changes occur in regions occupied by the key residues: Thr236 (side-chain and backbone oxygen atoms), Ser218 (side-chain oxygen atom), and Wat623 (water), which shows that these groups are well-positioned to stabilize the TS. Red areas on the differential electrostatic potential-colored surface are accompanied by short contacts between oxygen atoms of these residues and the reaction center, implying that these oxygen atoms are important for lowering the activation barrier. The three residues discussed here may also be involved in hydrogen bonding with prospective inhibitors. Finally, an

Table 2. Interaction Energies between the FAAH-Oleamide Reaction Model and Its Enzymatic Environment at Various Levels of Theory, As Defined by Equation 2[a]

	sum of pairwise interactions				supermolecule environment			
	Δ_{EL}	Δ_{HL}	Δ_{SCF}	Δ_{MP2}	Δ_{EL}	Δ_{HL}	Δ_{SCF}	Δ_{MP2}
substrate	−64.7	18.6	−3.2	−25.4	−68.4	11.9	−12.0	−34.9
transition state	−88.0	9.3	−24.2	−46.5	−92.1	1.9	−34.9	−58.4
DTSS	**−23.3**	**−9.3**	**−21.0**	**−21.1**	**−23.7**	**-10.0**	**−22.9**	**−23.5**

[a]Polarization effects among residues are largely responsible for the differences between the left (pair-wise interactions between single residues) and the right (interactions for the entire active site model) sides of the Table. All values are in kilocalories per mole. The counterpoise correction was applied throughout, although basis set extension effects due to different basis set sizes of the pair-wise and supermolecule models were not considered. This may be responsible for minor DTSS differences observed between the two models.

dx.doi.org/10.1021/jp401834v | J. Phys. Chem. B 2013, 117, 6656–6666

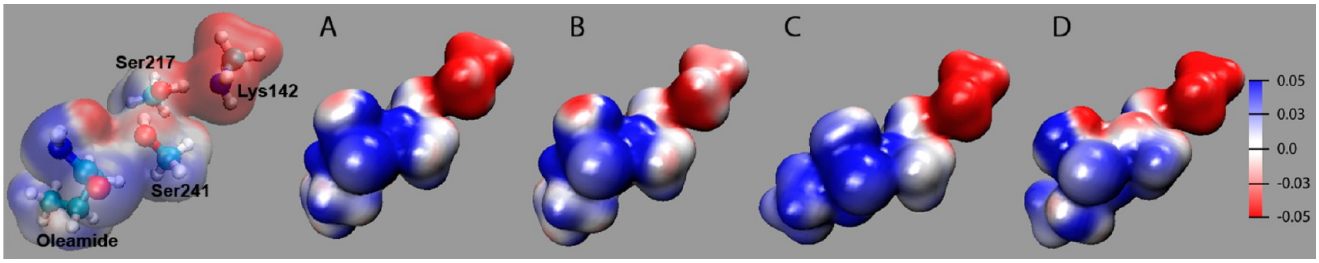

Figure 7. Catalytic fields around the reaction centers of the four conformations from ref 17. Positive (negative) electrostatic potential differences in the reacting system are associated with red (blue) according to the scale on the right-hand side (in au). The sign of the differential potential, visualized on the electronic isodensity surface of 0.01 au, is inverted to show the optimal electrostatic characteristics of a complementary molecular environment.

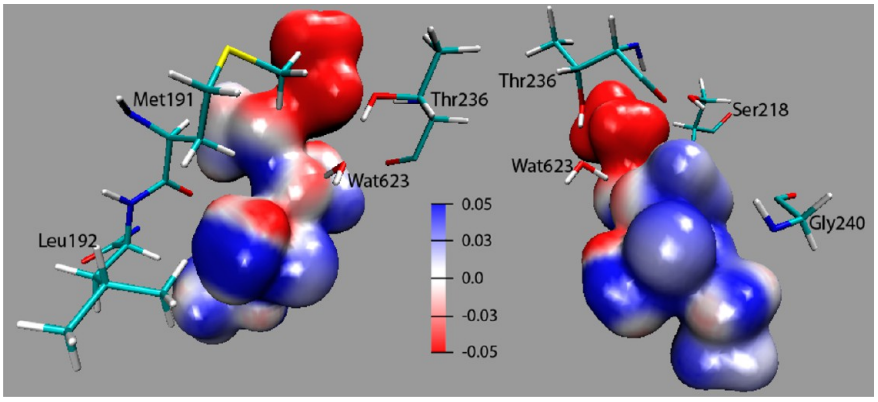

Figure 8. Catalytic field (differential electrostatic potential in au) mapped onto the electronic isodensity surface of 0.01 au around the reaction center of conformation D (the catalytic triad Lys142- Ser217-Ser241 and oleamide up to C4). Selected catalytic residues identified by DTSS analysis are also shown for context.

important role can be attributed to the backbone oxygen atom of Met191, which is involved in hydrogen bonding with the oleamide amino group.

Multiple Sequence Alignment. Differential stabilization of the TS, which corresponds to lowering the activation barrier, is important for FAAH catalysis. We therefore examined whether residues identified as stabilizing the TS and having an effect on the reaction for rat FAAH are present in other species, including humans. To that end, multiple sequence alignment was performed, the results of which are presented in Figure 9. The catalytic triad (Lys142, Ser217, and Ser241), found in members of the amidase signature family, is conserved among all of the species analyzed. A high degree of evolutionary conservation is also seen for other residues associated with pronounced DTSS effects, both stabilizing and destabilizing, especially Ser218, Gly216, Thr236, Asn237, Ile238, Gly239, Gly240, and Arg243. Some amino acid side chains are interchanged: Thr/Ser (218, 236), Ile/Val/Leu (238), and Gly/Ala(239). The fact that these swapping residues are quite similar is significant because one would expect evolutionary adaptation to retain the necessary type of enzyme−substrate/TS interaction. Multiple sequence alignment also shows the following highly conserved regions around the catalytic triad, which were not included into the DTSS analysis due to further distance from the reaction center: from Pro/His138 to Asp/Glu142 and then from Gly215 to Arg/Lys255.

Inhibitor Studies. Three FAAH inhibitors belonging to the class of cyclohexyl carbamic acid biphenyl-3-yl esters, namely, URB524, URB694, and URB618 (Figure 10), were also analyzed with DTSS and the variation−perturbation interaction energy decomposition scheme.[41,42] All three of these inhibitors are "false substrates" for this enzyme, meaning that they are cleaved by FAAH following a mechanism similar to oleamide hydrolysis with Ser241 acting as a nucleophile.[43,44] As previously described,[42] the carbamate inhibitors may select different binding modes; however, the reactive conformation gives the lowest activation energy barrier. This reaction, modeled analogously to the FAAH−oleamide reaction, showed similar binding to the natural substrate, including the oxyanion hole.[42] Instead of forming a transient acylenzyme, however, these carbamates form carbamoylenzymes, which are resistant to hydrolysis and thus responsible for FAAH inhibition.[45]

DTSS calculations show that conserved residues in the FAAH active site also play an important role in the TS stabilization for carbamoylation (Figure 11). Thr236 and Ser218, which are responsible for hydrogen bonding to Lys142, are the most important residues during the reaction with these covalent inhibitors. Residues of the oxyanion hole (Ile238, Gly239, and Gly240) also strongly influence TS stabilization, as does Arg243 and the conserved water Wat623. Backbone carbonyl of Met191 accepts a hydrogen bond from the amide group of oleamide and exhibits a much weaker effect due to the absence of this group in the carbamate inhibitors structures. Variation−perturbation interaction energy decomposition performed for the inhibitor reaction further confirms the dominant role of the multipole electrostatic energy, which corresponds to MP2 results with a correlation coefficient of 0.95, 0.96, and 0.99 for URB524, URB694, and URB618, respectively (Tables SI-5−SI-7 in the Supporting Information).

We also adopted the catalytic field approach to investigate the cleavage reactions of these covalent inhibitors. The catalytic fields for URB524, URB694 and URB618 around the catalytic

dx.doi.org/10.1021/jp401834v | J. Phys. Chem. B 2013, 117, 6656−6666

SIMULATION_SEQUENCE	36	PVSLKECFS	110	PGGSSGGEGAL	130	LGTDIGGSIRF
FAAH_Neosartorya_fischeri	3680	PISIKDGFE	3756	SGGSSGGEGAL	3776	VGTDIGGSIRI
FAAH_Ajellomyces_capsulatus	126	PISIKDGFE	202	SGGSSGGEGAL	222	VGTDIGGSIRI
A_Ajellomyces_dermatitidis	716	PLSLKDSFI	792	PGGSTGGEGAL	812	VGTDIAGSIRI
A_Cryptococcus_neoformans	2527	PLSLKDNFI	2603	PGGSSGGEGAI	2623	VGTDIGGSIRI
AC_Coccidioides_immitis	165	PISLKDTFT	241	PGGSSGGEGAI	261	VGTDIGGSIRI
FAAH_Ajellomyces_dermatitidis	131	PVSLKDNFN	207	PGGSSGGESAL	227	VGTDIGGSLRI
QtRNA_Paracoccidioides_brasiliensis	131	PISLKDNFN	207	SGGSSGGESAL	227	VGTDIGGSLRI
FAAH_Microsporum_canis	141	PVSIKDNFN	217	SGGSSGGESAL	237	VGTDIGGSLRI
AC_Talaromyces_stipitatus	1339	PISLKDNFN	1415	SGGSSGGESAL	1435	VGTDIGGSLRI
FAAH_Aspergillus_clavatus	140	PISIKDNFN	216	SGGSSGGESAL	236	VGTDIGGSLRI
AC_Emericella_unguis	123	PISLKDQLR	199	CGGSSGGEGAM	219	VGTDIGGSIRV
ACB_Aspergillus_ustus	125	PVSLKDQLR	199	CGGSSGGEGAL	219	VGTDIGGSIRV
AC_Monascus_purpureus	125	PISLKDQLR	201	CGGSSGGEGAM	221	VGTDIGGSIRV
AC_Pichia_stipitis	132	PISLKDNFN	210	SGGSSGGEAAL	230	IGSDIGGSIRI
AC_Paracoccidioides_brasiliensis	128	PVSLKDQFN	204	PGGSSGGESAL	224	FGTDIGGSIRI
AFP_Tetrahymena_thermophila	772	PVSLKDQFN	848	PGGSSGGESAL	868	FGTDIGGSIRI
AC_Ajellomyces_capsulatus	128	PVTLKDQFN	204	SGGSTGGENAL	224	IGTDIGGSIRI
AFP_Coccidioides_posadasii	154	PISLKDQFN	230	PGGSTGGEAAL	250	FGTDIGGSIRI
AC_Aspergillus_flavus	695	PVTLKDQFN	771	PGGSTGGEGAL	791	FGTDIGGSIRI
AC_Neosartorya_fischeri	129	PVTLKDQFN	205	PGGSTGGEGAL	225	FGTDIGGSVRI
FAAH_Tetrahymena_thermophila	792	PVTLKDQFN	868	PGGSTGGEGAL	888	FGTDIGGSIRI
AC_Aspergillus_clavatus	128	PITLKDQFN	204	PGGSTGGEAAL	224	LGTDIGGSIRI
AC_Penicillium_marneffei	129	PITLKDQFN	205	SGGSTGGEAAL	225	FGTDIGGSIRI
AP_Ustilaginoidea_virens	108	PVSLKDTID	184	PGGSTGGEGAL	203	IGSDVAGSVRC
AC_Verticillium_albo-atrum	108	PVSLKDSLH	184	PGGSTGGESAL	203	IGSDVAGSVRV
AC_Pyrenophora_tritici-repentis	108	PVSLKDSVH	184	PGGSTGGESAL	204	IGSDVAGSVRA
vit_D3_Paracoccidioides_brasiliensis	102	PVSLKDSFQ	178	PGGSTGGEAAL	197	IGSDVAGSVRV
AP_Paracoccidioides_brasiliensis	113	PVSLKDSFQ	189	PGGSTGGEAAL	208	IGSDVAGSVRV
A_Ajellomyces_capsulatus	731	PVSLKDSLQ	807	PGGSTGGEAAL	826	IGSDVAGSVRV
AC_Ajellomyces_dermatitidis	728	PVSLKDSIH	804	PGGSSGGEGAI	823	VGSDVAGSVRV
AC_Microsporum_canis	109	PVSLKDSIQ	185	PGGSSGGEASL	204	VGSDVAGSVRL
AC_Aspergillus_fumigatus	109	PVSLKDSVQ	185	PGGSTGGEGAL	204	IGSDVAGSVRV
FAAH_Rattus_norvegicus	138	PVSLKECFS	214	PGGSSGGEGAL	234	LGTDIGGSIRF
FAAH_Mus_musculus	138	PVSLKECFS	214	PGGSSGGEGAL	234	LGTDIGGSIRF
FAAH_Bos_taurus	138	HVSLKECFS	214	PGGSSGGEGAL	234	LGTDIGGSIRF
FAAH_Homo_sapiens	138	PVSLKECFT	214	PGGSSGGEGAL	234	LGTDIGGSIRF
FAAH_Sus_scrofa	138	PVSLKECFS	214	PGGSSGGEGAL	234	LGTDIGGSIRF
FAAH_Mesocricetus_auratus	33	PVSLKECFS	109	PGGSSGGEGAL	129	LGTDIGGSIRF
vit_D3_Gallus_gallus	146	PVSIKDHID	222	PGGSSGGEGAL	242	IGSDVAGSIRL
A_Schistosoma_mansoni	162	PISIKEGIA	238	PGGSSSGEAVL	258	IGTDIAGSIRI
A_Brugia_malayi	661	PISIKEGIA	737	PGGSSSGEAVL	757	IGTDIAGSIRI
FAAH_Schistosoma_mansoni	171	PVSLKELCS	247	TGGSSSGEGVL	267	IGTDLAGSIRI

Figure 9. Multiple sequence alignment in the proximity of the catalytic triad (Lys142-Ser217-Ser241 residues shown in green) from the amidase signature family. Some of the most important residues that stabilize (Ser218, Thr236, Ile238, Gly239, Gly240, Arg243) or destabilize (Gly216, Asp237) the transition state are shown in blue and yellow, respectively. Abbreviations: vit_D3 – vitamin D3 hydroxylase-associated protein; QtRNA, glutamyl-tRNA(gln) amidotransferase; FAAH, fatty acid amide hydrolase; AC, acetamidase; AP, amidase protein; A, amidase; AFP, amidase family protein; and ACB, acetamidase-B. Residues in all sequences are numbered according to the first deposited FAAH amino acid sequence of *Rattus norvegicus* (the common rat).

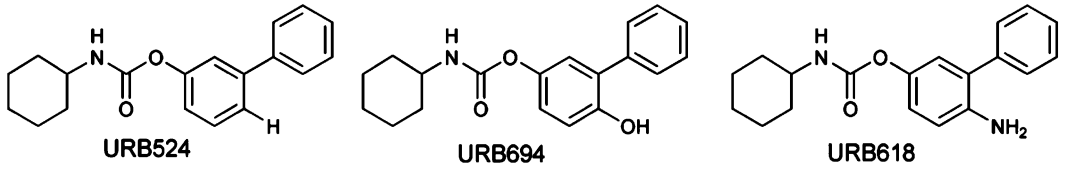

Figure 10. FAAH inhibitors considered in this study. URB524, the reference inhibitor, was substituted with *p*-hydroxy (URB694) and *p*-amino (URB618) groups to obtain the other two.

triad (Figure 12) are qualitatively similar to that the field found for the reactive conformation D for oleamide acylation (Figure 8). Slightly different catalytic environments are optimal for each compound, with the largest differences around the *p*-hydroxy and *p*-amino groups. URB524 and URB694 exhibit similar catalytic fields, with minor deformations around the hydroxyl group of URB694. URB618 carries a strong positive potential on its proximal phenyl ring, caused by a basic aniline nitrogen atom that would be optimally stabilized by a positive environment.

Such catalytic fields exemplify the electronic structure changes that occur in the reactants and the TS during the reaction. Visualizing these changes allows one to quickly identify regions of the FAAH inhibitor adducts, where significant electronic charge redistribution takes place. There are two, namely, the alkyl substituent at the nitrogen atom and the distal phenyl ring of the biphenyl moiety. Calculations thus indicate that these two areas are the most important for modulating interactions between FAAH and carbamate derivatives, in agreement with previous SAR data[21,22] (Figure 13).

■ CONCLUSIONS

In this work, we have investigated the catalytic activity of FAAH in terms of DTSS, with the aim of determining which residues affect the activation energy barrier the most. Interaction energies were calculated at the MP2 level for four previously identified reactant conformations A, B, C, and D taken from QM/MM calculations.[17] Energies obtained from a pairwise interaction energy approximation were validated by a supermolecule model. Further decomposition of the MP2 interaction energies demonstrated the dominant electrostatic nature of FAAH active site interactions, justifying in turn a catalytic field approach that clearly illustrates the differences between the four conformations. The results were also compared with available

dx.doi.org/10.1021/jp401834v | J. Phys. Chem. B 2013, 117, 6656–6666

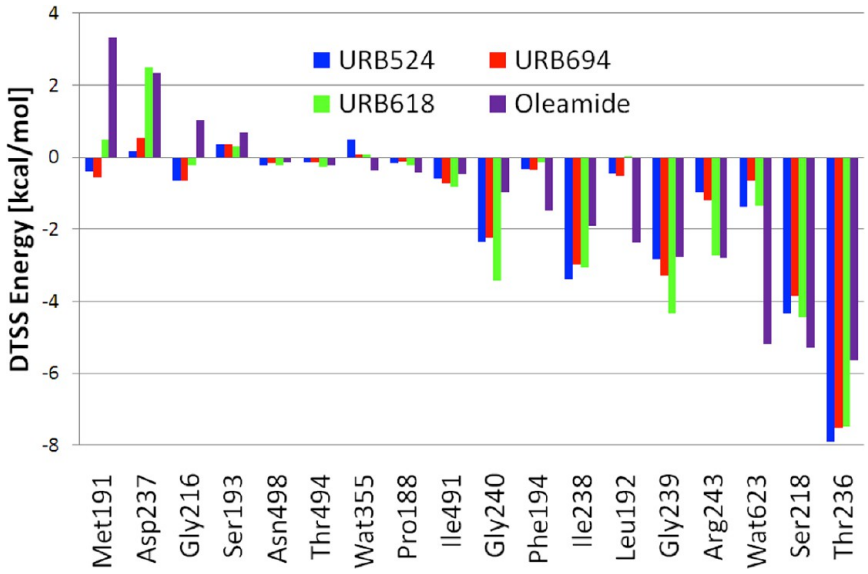

Figure 11. DTSS effects calculated at the MP2 level of theory for the reactions with inhibitors[42] (URB524, URB694, and URB618) and for the reactive conformation D of oleamide. Increasing TS stabilization contributions in oleamide acylation ranks FAAH active-site components.

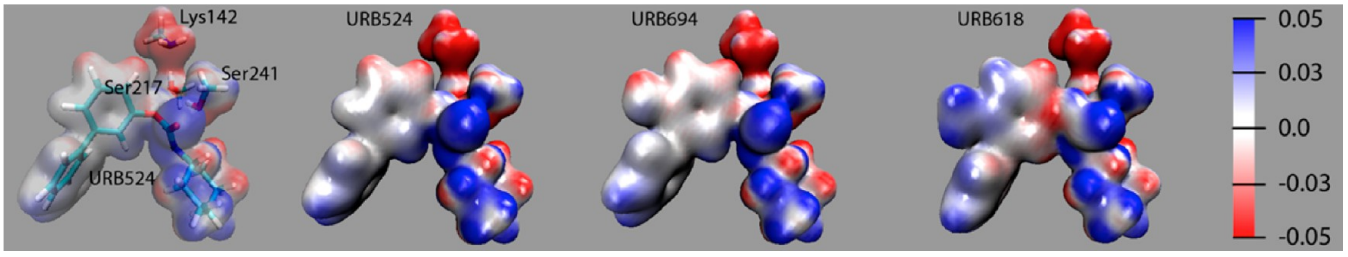

Figure 12. Catalytic fields around the URB524, URB694, and URB618 reaction centers, consisting of the Lys142-Ser217-Ser241 catalytic triad and a single inhibitor. Positive and negative values of the electrostatic potential (in au) are mapped onto the 0.01 au electronic isodensity surface.

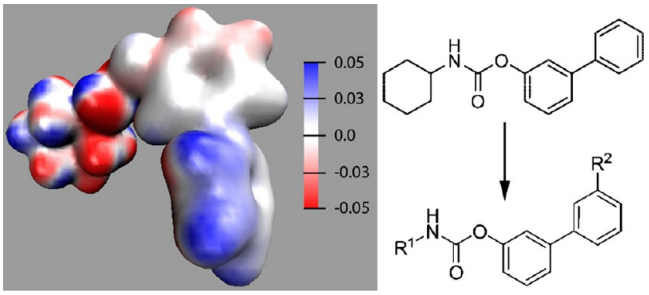

Figure 13. Catalytic field around the URB524 inhibitor and the chemical structure of the inhibitor. The compound was substituted (arrow) in positions R^1 and R^2 based on the structure–activity relationships constructed in refs 21 and 22.

experimental data, including multiple sequence alignment, site-directed mutagenesis, and reactions with inhibitors.

The computations reported here determine key stabilizing residues for the TS of oleamide hydrolysis, namely, Thr236, Ser218, and Wat623 (a conserved water molecule). Smaller contributions also arise from Arg243, Gly239, Leu192, Ile238, Phe194, and Gly240. Furthermore, the activation energy barriers of the four conformations (A–D) correlate with DTSS energies, and the strongest TS stabilization was found for conformation D, which was previously identified as the most reactive one.[17] This agreement highlights the importance of TS stabilization for the efficiency of reactions proceeding in FAAH.

The nonempirical analysis here supports the conclusions from QM/MM calculations, indicating that the QM/MM method provides a good description of the FAAH reaction. Interaction energy decomposition confirms that the electrostatic component is dominant within the FAAH active site, and we illustrate the differences between conformations using a catalytic field approach. Multiple sequence alignment in turn provides evidence that the residues promoting TS formation are conserved in the amidase signature family. The importance of the residues involved in oleamide acylation has been confirmed for URB524, URB618, and URB694 inhibitors, which provides an insight into future inhibitor design.

■ ASSOCIATED CONTENT

Ⓢ Supporting Information

Detailed interaction energies for conformations A, B, C, and D and the carbamate-based inhibitors as well as the Cartesian coordinates of the active site model for the reactive D conformation. This material is available free of charge via the Internet at http://pubs.acs.org.

■ AUTHOR INFORMATION

Corresponding Author

*E-mail: Andrzej.Sokalski@pwr.wroc.pl; Adrian.Mulholland@bristol.ac.uk.

Notes

The authors declare no competing financial interest.

■ ACKNOWLEDGMENTS

E.I.C. and A.J.M. thank the U.K. Engineering and Physical Science Research Council (grant number EP/G007705/1) for support. A.J.M. is an Engineering and Physical Science Research Council Leadership Fellow. This work was also financed by a statutory activity subsidy from Polish Ministry of Science and Higher Education for the Faculty of Chemistry of Wroclaw University of Technology. The Royal Thai Government is also acknowledged for funding (J.S.). Most of the calculations were performed at Wroclaw Centre for Networking and Supercomputing (WCSS).

■ REFERENCES

(1) Pauling, L. Molecular Architecture and Biological Reactions. *Chem. Eng. News Archive* **1946**, *24*, 1375−1377.
(2) Warshel, A.; Sharma, P. K.; Kato, M.; Parson, W. W. Modeling Electrostatic Effects in Proteins. *Biochim. Biophys. Acta* **2006**, *1764*, 1647−1676.
(3) Warshel, A.; Sharma, P. K.; Kato, M.; Xiang, Y.; Liu, H.; Olsson, M. H. M. Electrostatic Basis for Enzyme Catalysis. *Chem. Rev.* **2006**, *106*, 3210−3235.
(4) Chebrou, H.; Bigey, F.; Arnaud, A.; Galzy, P. Study of the Amidase Signature Group. *Biochim. Biophys. Acta* **1996**, *1298*, 285−293.
(5) Patterson, J. E.; Ollmann, I. R.; Cravatt, B. F.; Boger, D. L.; Wong, C.-H.; Lerner, R. A. Inhibition of Oleamide Hydrolase Catalyzed Hydrolysis of the Endogenous Sleep-Inducing Lipid cis-9-Octadecenamide. *J. Am. Chem. Soc.* **1996**, *118*, 5938−5945.
(6) Cravatt, B. F.; Demarest, K.; Patricelli, M. P.; Bracey, M. H.; Giang, D. K.; Martin, B. R.; Lichtman, A. H. Supersensitivity to Anandamide and Enhanced Endogenous Cannabinoid Signaling in Mice Lacking Fatty Acid Amide Hydrolase. *Proc. Natl. Acad. Sci. U.S.A.* **2001**, *98*, 9371−9376.
(7) Cravatt, B. F.; Giang, D. K.; Mayfield, S. P.; Boger, D. L.; Lerner, R. A.; Gilula, N. B. Molecular Characterization of an Enzyme that Degrades Neuromodulatory Fatty-acid Amides. *Nature* **1996**, *384*, 83−87.
(8) Wilson, R. I.; Nicoll, R. A. Endocannabinoid Signaling in the Brain. *Science* **2002**, *296*, 678−682.
(9) Solorzano, C.; Zhu, C.; Battista, N.; Astarita, G.; Lodola, A.; Rivara, S.; Mor, M.; Russo, R.; Maccarrone, M.; Antonietti, F.; et al. Selective N-Acylethanolamine-Hydrolyzing Acid Amidase Inhibition Reveals a Key Role for Endogenous Palmitoylethanolamide in Inflammation. *Proc. Natl. Acad. Sci. U.S.A.* **2009**, *106*, 20966−20971.
(10) Fu, J.; Gaetani, S.; Oveisi, F.; Verme, J. L.; Serrano, A.; Fonseca, F. R. de; Rosengarth, A.; Luecke, H.; Giacomo, B. D.; Tarzia, G.; et al. Oleylethanolamide Regulates Feeding and Body Weight through Activation of the Nuclear Receptor PPAR-α. *Nature* **2003**, *425*, 90−93.
(11) Bisogno, T.; De Petrocellis, L.; Di Marzo, V. Fatty Acid Amide Hydrolase, an Enzyme with Many Bioactive Substrates. Possible Therapeutic Implications. *Curr. Pharm. Des.* **2002**, *8*, 533−547.
(12) Cravatt, B. F.; Prospero-Garcia, O.; Siuzdak, G.; Gilula, N. B.; Henriksen, S. J.; Boger, D. L.; Lerner, R. A. Chemical Characterization of a Family of Brain Lipids That Induce Sleep. *Science* **1995**, *268*, 1506−1509.
(13) Cravatt, B. F.; Lerner, R. A.; Boger, D. L. Structure Determination of an Endogenous Sleep-Inducing Lipid, cis-9-Octadecenamide (Oleamide): A Synthetic Approach to the Chemical Analysis of Trace Quantities of a Natural Product. *J. Am. Chem. Soc.* **1996**, *118*, 580−590.
(14) Labar, G.; Michaux, C. Fatty Acid Amide Hydrolase: From Characterization to Therapeutics. *Chem. Biodiversity* **2007**, *4*, 1882−1902.
(15) Bracey, M. H.; Hanson, M. A.; Masuda, K. R.; Stevens, R. C.; Cravatt, B. F. Structural Adaptations in a Membrane Enzyme That Terminates Endocannabinoid Signaling. *Science* **2002**, *298*, 1793−1796.
(16) Lodola, A.; Mor, M.; Hermann, J. C.; Tarzia, G.; Piomelli, D.; Mulholland, A. J. QM/MM Modelling of Oleamide Hydrolysis in Fatty Acid Amide Hydrolase (FAAH) Reveals a new Mechanism of Nucleophile Activation. *Chem. Commun.* **2005**, 4399.
(17) Lodola, A.; Mor, M.; Zurek, J.; Tarzia, G.; Piomelli, D.; Harvey, J. N.; Mulholland, A. J. Conformational Effects in Enzyme Catalysis: Reaction via a High Energy Conformation in Fatty Acid Amide Hydrolase. *Biophys. J.* **2007**, *92*, L20−L22.
(18) Lodola, A.; Sirirak, J.; Fey, N.; Rivara, S.; Mor, M.; Mulholland, A. J. Structural Fluctuations in Enzyme-Catalyzed Reactions: Determinants of Reactivity in Fatty Acid Amide Hydrolase from Multivariate Statistical Analysis of Quantum Mechanics/Molecular Mechanics Paths. *J. Chem. Theory Comput.* **2010**, *6*, 2948−2960.
(19) Capoferri, L.; Mor, M.; Sirirak, J.; Chudyk, E.; Mulholland, A.; Lodola, A. Application of a SCC-DFTB QM/MM Approach to the Investigation of the Catalytic Mechanism of Fatty Acid Amide Hydrolase. *J. Mol. Model.* **2011**, *17*, 2375−2383.
(20) Tubert-Brohman, I.; Acevedo, O.; Jorgensen, W. L. Elucidation of Hydrolysis Mechanisms for Fatty Acid Amide Hydrolase and Its Lys142Ala Variant via QM/MM Simulations. *J. Am. Chem. Soc.* **2006**, *128*, 16904−16913.
(21) Mor, M.; Rivara, S.; Lodola, A.; Plazzi, P. V.; Tarzia, G.; Duranti, A.; Tontini, A.; Piersanti, G.; Kathuria, S.; Piomelli, D. Cyclohexylcarbamic Acid 3′- or 4′-Substituted Biphenyl-3-yl Esters as Fatty Acid Amide Hydrolase Inhibitors: Synthesis, Quantitative Structure−Activity Relationships, and Molecular Modeling Studies. *J. Med. Chem.* **2004**, *47*, 4998−5008.
(22) Mor, M.; Lodola, A.; Rivara, S.; Vacondio, F.; Duranti, A.; Tontini, A.; Sanchini, S.; Piersanti, G.; Clapper, J. R.; King, A. R.; et al. Synthesis and Quantitative Structure−Activity Relationship of Fatty Acid Amide Hydrolase Inhibitors: Modulation at the N-Portion of Biphenyl-3-yl Alkylcarbamates. *J. Med. Chem.* **2008**, *51*, 3487−3498.
(23) McKinney, M. K.; Cravatt, B. F. Evidence for Distinct Roles in Catalysis for Residues of the Serine-serine-lysine Catalytic Triad of Fatty Acid Amide Hydrolase. *J. Biol. Chem.* **2003**, M303922200.
(24) Patricelli, M. P.; Cravatt, B. F. Clarifying the Catalytic Roles of Conserved Residues in the Amidase Signature Family. *J. Biol. Chem.* **2000**, *275*, 19177−19184.
(25) Patricelli, M. P.; Cravatt, B. F. Fatty Acid Amide Hydrolase Competitively Degrades Bioactive Amides and Esters through a Nonconventional Catalytic Mechanism. *Biochemistry* **1999**, *38*, 14125−14130.
(26) Patricelli, M. P.; Lovato, M. A.; Cravatt, B. F. Chemical and Mutagenic Investigations of Fatty Acid Amide Hydrolase: Evidence for a Family of Serine Hydrolases with Distinct Catalytic Properties. *Biochemistry* **1999**, *38*, 9804−9812.
(27) Sokalski, W. A. The Physical Nature of Catalytic Activity due to the Molecular Environment in Terms of Intermolecular Interaction Theory: Derivation of Simplified Models. *J. Mol. Catal.* **1985**, *30*, 395−410.
(28) Szefczyk, B.; Mulholland, A. J.; Ranaghan, K. E.; Sokalski, W. A. Differential Transition-State Stabilization in Enzyme Catalysis: Quantum Chemical Analysis of Interactions in the Chorismate Mutase Reaction and Prediction of the Optimal Catalytic Field. *J. Am. Chem. Soc.* **2004**, *126*, 16148−16159.
(29) Szarek, P.; Dyguda-Kazimierowicz, E.; Tachibana, A.; Sokalski, W. A. Physical Nature of Intermolecular Interactions within cAMP-Dependent Protein Kinase Active Site: Differential Transition State Stabilization in Phosphoryl Transfer Reaction. *J. Phys. Chem. B* **2008**, *112*, 11819−11826.
(30) Sokalski, W. A.; Roszak, S.; Pecul, K. An Efficient Procedure for Decomposition of the SCF Interaction Energy into Components with Reduced Basis set Dependence. *Chem. Phys. Lett.* **1988**, *153*, 153−159.
(31) *Computational Approaches to Biochemical Reactivity*, 1st ed.; Náray-Szabó, G., Warshel, A., Eds.; Kluwer Academic Publishers: Dordrecht, The Netherlands, 1997.
(32) Dyguda-Kazimierowicz, E.; Sokalski, W.; Leszczyński, J. Non-empirical Study of the Phosphorylation Reaction Catalyzed by 4-

methyl-5-β-hydroxyethylthiazole Kinase: Relevance of the Theory of Intermolecular Interactions. *J. Mol. Model.* **2007**, *13*, 839−849.
(33) Boys, S. F.; Bernardi, F. The Calculation of Small Molecular Interactions by the Differences of Separate Total Energies. Some Procedures with Reduced Errors. *Mol. Phys.* **1970**, *19*, 553−566.
(34) Frisch, M. J.; Trucks, G. W.; Schlegel, H. B.; Scuseria, G. E.; Robb, M. A.; Cheeseman, J. R.; Montgomery, J. A., Jr.; Vreven, T.; Kudin, K. N.; Burant, J. C.; et al. *Gaussian 03*, revision C.02.; Gaussian, Inc.: Wallingford, CT, 2004.
(35) Humphrey, W.; Dalke, A.; Schulten, K. VMD: Visual Molecular Dynamics. *J. Mol. Graph.* **1996**, *14*, 33−38.
(36) Altschul, S. F.; Gish, W.; Miller, W.; Myers, E. W.; Lipman, D. J. Basic Local Alignment Search Tool. *J. Mol. Biol.* **1990**, *215*, 403−410.
(37) Larkin, M. A.; Blackshields, G.; Brown, N. P.; Chenna, R.; McGettigan, P. A.; McWilliam, H.; Valentin, F.; Wallace, I. M.; Wilm, A.; Lopez, R.; et al. Clustal W and Clustal X version 2.0. *Bioinformatics* **2007**, *23*, 2947−2948.
(38) Gora, R.; Roszak, S.; Sokalski, W. A.; Leszczynski, J. *Jackson State University Preprint*, 1999.
(39) Schmidt, M. W.; Baldridge, K. K.; Boatz, J. A.; Elbert, S. T.; Gordon, M. S.; Jensen, J. H.; Koseki, S.; Matsunaga, N.; Nguyen, K. A.; Su, S.; et al. General Atomic and Molecular Electronic Structure System. *J. Comput. Chem.* **1993**, *14*, 1347−1363.
(40) Štrajbl, M.; Florián, J.; Warshel, A. Ab Initio Evaluation of the Potential Surface for General Base- Catalyzed Methanolysis of Formamide: A Reference Solution Reaction for Studies of Serine Proteases. *J. Am. Chem. Soc.* **2000**, *122*, 5354−5366.
(41) Lodola, A.; Capoferri, L.; Rivara, S.; Chudyk, E.; Sirirak, J.; Dyguda-Kazimierowicz, E.; Sokalski, W. A.; Mileni, M.; Tarzia, G.; Piomelli, D.; et al. Understanding the Role of Carbamate Reactivity in Fatty Acid Amide Hydrolase Inhibition by QM/MM Mechanistic Modelling. *Chem. Commun.* **2011**, *47*, 2517−2519.
(42) Lodola, A.; Mor, M.; Rivara, S.; Christov, C.; Tarzia, G.; Piomelli, D.; Mulholland, A. J. Identification of Productive Inhibitor Binding Orientation in Fatty Acid Amide Hydrolase (FAAH) by QM/MM Mechanistic Modelling. *Chem. Commun.* **2008**, 214−216.
(43) Tarzia, G.; Duranti, A.; Gatti, G.; Piersanti, G.; Tontini, A.; Rivara, S.; Lodola, A.; Plazzi, P. V.; Mor, M.; Kathuria, S.; et al. Synthesis and Structure−Activity Relationships of FAAH Inhibitors: Cyclohexylcarbamic Acid Biphenyl Esters with Chemical Modulation at the Proximal Phenyl Ring. *ChemMedChem* **2006**, *1*, 130−139.
(44) Alexander, J. P.; Cravatt, B. F. Mechanism of Carbamate Inactivation of FAAH: Implications for the Design of Covalent Inhibitors and In Vivo Functional Probes for Enzymes. *Chem Biol* **2005**, *12*, 1179−1187.
(45) Keith, J. M.; Apodaca, R.; Xiao, W.; Seierstad, M.; Pattabiraman, K.; Wu, J.; Webb, M.; Karbarz, M. J.; Brown, S.; Wilson, S.; et al. Thiadiazolopiperazinyl Ureas as Inhibitors of Fatty Acid Amide Hydrolase. *Bioorg. Med. Chem. Lett.* **2008**, *18*, 4838−4843.